Contribution from the Department of Medicinal Chemistry, Hiroshima University School of Medicine, Kasumi, Minami-ku, Hiroshima 734, Japan, Department of Chemistry, College of General Education, Hirosaki University, Bunkyo, Hirosaki 036, Japan, and Faculty of Pharmaceutical Sciences, University of Tokyo, Hongo, Bunkyo-ku, Tokyo 113, Japan

New-Dimensional Cyclam. Synthesis, Crystal Structure, and Chemical Properties of Macrocyclic Tetraamines Bearing a Phenol Pendant

Eiichi Kimura,*† Tohru Koike,† Keiji Uenishi,† Markus Hediger,† Miyuki Kuramoto,† Shuzo Joko,† Yoko Arai,† Mutsuo Kodama,‡ and Yoichi Iitaka§

Received April 15, 1987

Newly devised 13–15-membered macrocyclic tetraamine (N_4) ligands attached with a phenolic pendant (**10**, **11**, **13**, and **15**) have been synthesized to determine the influence of the phenol on the cation-enclosure properties of the macrocyclic N_4 and, conversely, the influence of the proximate cations encompassed in N_4 macrocycles on the chemical behavior of the phenolate pendant. The synthesis involves a novel annelation reaction between coumarin and suitable tetraamines. The favorable location of phenol in the periphery of the macrocycle has been confirmed by the X-ray crystal structure of the phenol-pendant 14-membered N_4 (cyclam) **11b**. Dissociation of the phenolic protons is facilitated by incorporation of metal ions into the macrocycle, and the resulting phenolate ion atop stabilizes otherwise unstable complexes. The crystal structures of **11b** and its Cu^{II} complex **17a** have been determined. The crystals of **11b** ($C_{16}H_{28}N_4O$) are monoclinic, space group $P2_1/a$, with four molecules in the unit cell of dimensions a = 15.335 (8) Å, b = 8.535 (5) Å, c = 13.331 (7) Å, and β = 105.17 (5)°. Crystals of **17a**(ClO_4)·H_2O ($C_{16}H_{27}N_4OCuClO_4 \cdot H_2O$) are also monoclinic, space group $P2_1/n$, with four molecules in the unit cell of dimensions a = 30.943 (20) Å, b = 8.188 (4) Å, c = 7.936 (4) Å, and β = 95.89 (5)°. The structures were solved by the direct method for **11b** and the heavy-atom method for **17a** and refined by block-diagonal least-squares calculations: for **11b**, R = 0.061 for 2635 independent reflections, and for **17a**, R = 0.066 for 3703 independent reflections. The five-coordinate, square-pyramidal geometry around copper is illustrated with the phenolate oxygen at nearly the apex of the pyramid. The pH-metric and polarographic titration of Cu^{II}–**11b** revealed a complexation constant ($[CuH_{-1}L^+]/[Cu^{II}][H_{-1}L^-]$) of 1.0×10^{32} M^{-1} ($H_{-1}L$ is the phenolate species) and stability enhancement of $\sim 10^2$ by the phenolate coordination. Its strong σ donation contributes to stabilization of higher oxidation states of metal ions.

Saturated polyamine macrocycles possess cavities capable of providing a favorable environment for the reception of guest cation and anion species.[1] The strength of the ion binding is determined by ion size, macrocyclic cavity size, and ligand conformation.[2] Typically, the 14-membered tetraamine cyclam incorporates transition- and heavy-metal ions into its cavity to form stable, square-planar N_4 complexes with several configurations.[3]

The realization that the ion-binding characteristics of the macrocyclic ligand can be significantly modified by attaching additional binding sites to the periphery of the macrocycle has been an important feature of recent developments in macrocyclic chelates.[4] The molecular design, however, has not been extensive as yet both in synthetic tactics and in variation of additional donor functions. Few systems[5] have evolved in which the reception of guest cation species is triggered or facilitated by a reversible chemical change in a strategically placed new functional group. Were such synergism to occur, it might be revealed by a change in ion-binding characteristics or modified reactivity of the functional group.

We have now developed a novel synthetic method that yields the new series of macrocyclic tetraamines **11**, **13**, and **15** bearing a pendant phenolic group that is able to ideally project into the cavity. We have found that this phenolic group indeed influences the ion-incorporating properties of N_4 macrocycles and that, conversely, the chemical activity of the phenol functions attached to N_4 is changed.

The idea of apical phenolate coordination has come in part from an active center of catalases[6] or abnormal heme[7] that contain iron(III) complexes of square-planar macrocyclic N_4 porphyrins cofunctionalyzed with an apical phenolate donor from the surrounding proteins. Although a number of synthetic efforts have been made to intramolecularly attach an imidazole or other heterocyclic donors to porphyrins[8] or saturated N_4 macrocycles,[9] there were none that have disclosed the effect of the distinct apical coordination of phenol on the chemistry of square-planar N_4 complexes. Earlier communications briefly reported synthesis of the phenol-pendant cyclam **11b** from coumarin,[10] an X-ray structure of its Ni^{II} complex,[11] and the 13-membered N_4 complex with Ni^{II}.[12,13] Also reported was the phenol-pendant N_3 system.[14]

Experimental Section

General Methods. All materials were obtained commercially and were used without further purification. Melting points were determined by using a Yanako micro melting point apparatus and were uncorrected. UV–visible spectra were recorded on a Hitachi U-3200 double-beam spectrophotometer at 25.0 ± 0.1 °C using matched quartz cells of 2- or 10-mm path length, IR spectra on a Shimazu IR-408 spectrometer, ^1H NMR spectra on a Hitachi R-40 high-resolution NMR spectrometer (90 MHz, 35 °C, Me_4Si reference), and ^{13}C NMR spectra on a JEOL JNM-FX100S FT-NMR spectrometer (100 MHz, 22.5 °C, Me_4Si reference). Splitting patterns are indicated as follows: s, singlet; d, doublet, dd, AB quartet; m, multiplet. The ESR spectra were recorded on a JES-FE1X spectrometer using a small sample of MnO as reference at 77 K. For TLC analysis throughout this work, Merck precoated TLC plates (silica gel 60 F_{254}) were used.

Potentiometric Titrations. Aqueous solutions (50 mL) of ligands (1.00×10^{-3} M) with four equivalent $HClO_4$ groups were titrated with carbonate-free 0.100 M NaOH aqueous solution. pH values were read with an Orion 811 digital pH meter. The temperature was maintained at

† Hiroshima University School of Medicine.
‡ Hirosaki University.
§ University of Tokyo.

(1) Kimura, E. *Yuki Gosei Kagaku Kyokaishi* **1986**, *44*, 871–882.
(2) (a) Martin, L. Y.; DeHayes, L. J.; Zompa, L. J.; Busch, D. H. *J. Am. Chem. Soc.* **1974**, *96*, 4046–4048. (b) Thöm, V. J.; Fox, C. C.; Boeyens, J. C. A.; Hancock, R. D. *J. Am. Chem. Soc.* **1984**, *106*, 5947–5955.
(3) (a) Thöm, V. J.; Boeyens, J. C. A.; McDougall, G. J.; Hancock, R. D. *J. Am. Chem. Soc.* **1984**, *106*, 3198–3207. (b) Barefield, E. K.; Bianchi, A.; Billo, E. J.; Connolly, P. J.; Paoletti, P.; Summers, J. S.; Van Derveer, D. G. *Inorg. Chem.* **1986**, *25*, 4197–4202.
(4) Kimura, E. *Pure Appl. Chem.* **1986**, *58*, 1461–1466.
(5) Takagi, M.; Nakamura, H. *J. Coord. Chem.* **1986**, *15*, 53–82.
(6) Reid, T. J., III; Murthy, M. R. N.; Sicignano, A.; Tanaka, N.; Musick, W. D. L.; Rossmann, M. G. *Proc. Natl. Acad. Sci. U.S.A.* **1981**, *78*, 4767–4771.
(7) Pulsinelli, P. D.; Perutz, M. F.; Nagel, R. L. *Proc. Natl. Acad. Sci. U.S.A.* **1973**, *70*, 3870–3874.
(8) (a) Momenteau, M. *Pure Appl. Chem.* **1986**, *58*, 1493–1502. (b) Collman, J. P.; Brauman, J. I.; Doxsee, K. M.; Sessler, J. L.; Morris, R. M.; Gibson, Q. H. *Inorg. Chem.* **1983**, *22*, 1427–1432. (c) Traylor, T. G. *Acc. Chem. Res.* **1981**, *14*, 102–109.
(9) Kaden, T. A. *Top. Curr. Chem.* **1984**, *121*, 157.
(10) Kimura, E.; Koike, T.; Takahashi, M. *J. Chem. Soc., Chem. Commun.* **1985**, 385–386.
(11) Iitaka, Y.; Koike, T.; Kimura, E. *Inorg. Chem.* **1986**, *25*, 402–404.
(12) Kimura, E.; Uenishi, K.; Koike, T.; Iitaka, Y. *Chem. Lett.* **1986**, 1137–1140.
(13) Kimura, E.; Koike, T.; Uenishi, K.; Davidson, R. B. *J. Chem. Soc., Chem. Commun.* **1986**, 1110–1111.
(14) Kimura, E.; Yamaoka, M.; Morioka, M.; Koike, T. *Inorg. Chem.* **1986**, *25*, 3883–3886.

0020-1669/87/1326-2975$01.50/0

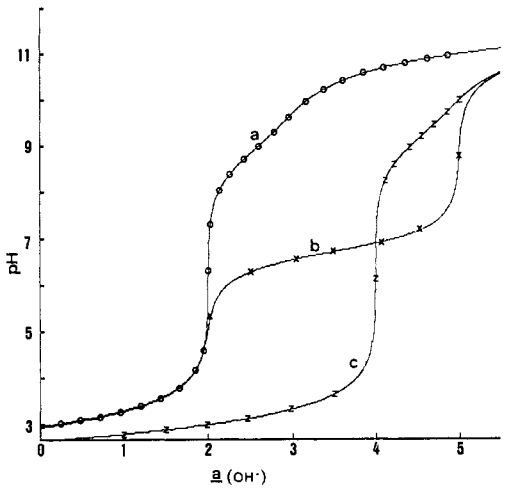

Figure 1. Calculated titration curves with the obtained values of pK_a, $K_{Fe^{II}H_{-1}L}$, and $K_{Cu^{II}H_{-1}L}$ (L = **11b**) from experimental values (○, ×, and z) for (a) 1.00×10^{-3} M **11b**·4$HClO_4$ and for (b) in the presence of 1.00×10^{-3} M Fe^{II} and (c) Cu^{II}.

Table I. Crystal Data and Data Collection Summary

	free ligand **11b**	Cu^{II} complex **17a**$(ClO_4)\cdot H_2O$
formula	$C_{16}H_{28}N_4O$	$C_{16}H_{27}N_4OCuClO_4\cdot H_2O$
M_r	292.4	472.4
cryst syst	monoclinic	monoclinic
space group	$P2_1/a$	$P2_1/n$
cryst color	colorless	blue
cell dimens		
a, Å	15.335 (8)	30.943 (20)
b, Å	8.535 (5)	8.188 (4)
c, Å	13.331 (7)	7.936 (4)
β, deg	105.17 (5)	95.89 (5)
V, Å^3	1684	2000
Z	4	4
calcd density, g cm^{-3}	1.153	1.569
cryst dimens, mm	0.3 × 0.3 × 0.1	0.2 × 0.2 × 1
radiation (graphite monochromated)	Cu Kα	Cu Kα
μ, cm^{-1}	5.52	31.3
2θ range, deg	6–156	6–156
scan speed, deg min^{-1}	6	6
phasing	direct method	heavy-atom method
no. of measd reflcns	2750	4579
no. of indep reflcns ($I > 2\sigma(I)$)	2635	3703
final R	0.061	0.066

25.00 ± 0.05 °C, and the ionic strength was adjusted to 0.10 M with $NaClO_4$. −log [H^+] values were estimated with a correction of −0.08 pH unit to the pH meter readings.[15] All the solutions were carefully protected from air by a stream of humidified argon. The electrode system was calibrated with pH 7.00 and 4.01 buffer solutions and checked by the duplicate theoretical titration curves of 4.00×10^{-3} M $HClO_4$ with a 0.100 M NaOH solution at 25 °C and I = 0.10 M ($NaClO_4$) in high- and low-pH regions. Calculated titration curves are shown in Figure 1 with the obtained values of pK_a and complex stability constants (for **17**) from experimental values.

Electrochemical Measurements. Cyclic voltammetry and dc polarography were performed with a Yanaco P-1100 polarographic analyzer system at 25.00 ± 0.05 °C. A three-electrode system was employed: a 3-mm glassy-carbon rod (Tokai Electrode Co. GC-30), a Yanagimoto P10-RE rotary glassy-carbon-disk electrode, or a Yanagimoto dropping mercury electrode as the working electrode, a Pt wire as the counter electrode, and a saturated calomel electrode (SCE) as the reference electrode. The cyclic voltammograms with scan rates of 10–100 mV s^{-1} and the dc polarograms with scan rates of 2–10 mV s^{-1} were evaluated graphically.

(15) *Kagaku Binran*, 3rd ed.; Chemical Society of Japan: Tokyo, 1984; Vol. II.
(16) Johnson, C. K. "ORTEP"; Report ORNL-3794; Oak Ridge National Laboratory: Oak Ridge, TN, 1965.

Table II. Final Fractional Coordinates (×10^4) for **11b** with Estimated Standard Deviations in Parentheses

atom	x	y	z	B_{eq}, Å^2
N(1)	4630 (1)	1928 (2)	4208 (2)	3.8 (0.0)
C(2)	5016 (2)	3224 (3)	3752 (2)	4.3 (0.0)
C(3)	5812 (2)	2658 (3)	3363 (2)	4.2 (0.0)
N(4)	5500 (1)	1514 (3)	2517 (2)	3.7 (0.0)
C(5)	6239 (2)	784 (3)	2154 (2)	3.9 (0.0)
C(6)	5855 (2)	−634 (4)	1449 (2)	4.9 (0.1)
C(7)	5513 (2)	−1993 (4)	1961 (2)	5.2 (0.1)
N(8)	4646 (2)	−1586 (3)	2162 (2)	4.5 (0.0)
C(9)	4244 (2)	−2882 (3)	2609 (2)	5.4 (0.1)
C(10)	3435 (2)	−2295 (4)	2958 (3)	5.8 (0.1)
N(11)	3741 (1)	−1137 (3)	3793 (2)	4.3 (0.0)
C(12)	2999 (2)	−278 (4)	4040 (3)	5.5 (0.1)
C(13)	3357 (2)	969 (4)	4866 (2)	5.2 (0.1)
C(14)	3795 (2)	2371 (4)	4484 (2)	4.7 (0.1)
C(15)	6643 (2)	1994 (3)	1570 (2)	3.8 (0.0)
C(16)	6106 (2)	3129 (4)	935 (2)	4.6 (0.0)
C(17)	6484 (2)	4207 (4)	390 (2)	5.4 (0.1)
C(18)	7399 (2)	4158 (4)	469 (3)	5.6 (0.1)
C(19)	7945 2)	3040 (4)	1082 (3)	5.4 (0.1)
C(20)	7558 (2)	1978 (4)	1626 (2)	4.4 (0.0)
O(21)	5196 (1)	3181 (3)	837 (2)	6.4 (0.0)

Table III. Final Fractional Coordinates (×10^4) for **17a**$(ClO_4)\cdot H_2O$ with Estimated Standard Deviations in Parentheses

atom	x	y	z	B_{eq}, Å^2
Cu	1152.4 (2)	2355.1 (9)	1541.1 (9)	2.54 (0.01)
N(1)	1066 (1)	3897 (5)	3489 (5)	2.9 (0.1)
C(2)	1435 (2)	3645 (7)	4808 (7)	3.4 (0.1)
C(3)	1835 (2)	3249 (7)	3953 (7)	3.2 (0.1)
N(4)	1731 (1)	1841 (5)	2803 (5)	2.6 (0.1)
C(5)	2077 (2)	1414 (6)	1712 (7)	2.9 (0.1)
C(6)	1935 (2)	−130 (7)	673 (7)	3.4 (0.1)
C(7)	1556 (2)	67 (7)	−685 (7)	3.4 (0.1)
N(8)	1145 (1)	325 (6)	53 (6)	3.3 (0.1)
C(9)	766 (3)	528 (13)	−1213 (12)	9.4 (0.2)
C(10)	476 (3)	1551 (16)	−990 (15)	13.3 (0.3)
N(11)	556 (1)	2802 (7)	351 (7)	4.3 (0.1)
C(12)	196 (2)	2867 (8)	1402 (9)	4.6 (0.1)
C(13)	264 (2)	4155 (8)	2774 (9)	4.4 (0.1)
C(14)	630 (2)	3803 (8)	4137 (8)	3.8 (0.1)
C(15)	2205 (1)	2827 (6)	607 (6)	2.7 (0.1)
C(16)	1903 (2)	3978 (7)	−182 (6)	2.9 (0.1)
C(17)	2077 (2)	5182 (7)	−1211 (7)	3.3 (0.1)
C(18)	2505 (2)	5220 (8)	−1473 (7)	3.7 (0.1)
C(19)	2795 (2)	4089 (8)	−722 (7)	3.6 (0.1)
C(20)	2639 (2)	2924 (7)	329 (7)	3.1 (0.1)
O(21)	1489 (1)	3952 (5)	−25 (5)	3.7 (0.1)
O(W)	869 (2)	6029 (9)	−1086 (7)	8.0 (0.1)
Cl	863 (1)	−1564 (2)	4239 (2)	4.2 (0.0)
O(1Cl)	1041 (2)	2 (6)	4583 (8)	7.8 (0.1)
O(2Cl)	1074 (4)	−2516 (12)	5648 (12)	6.5 (0.2)
O(2′Cl)	684 (6)	−2394 (15)	5458 (14)	11.0 (0.3)
O(3Cl)	420 (4)	−1619 (20)	4403 (18)	9.8 (0.3)
O(3′Cl)	516 (5)	−1226 (27)	3002 (23)	14.3 (0.5)
O(4Cl)	935 (6)	−2332 (12)	2762 (12)	10.1 (0.3)
O(4′Cl)	1216 (5)	−2306 (16)	3449 (23)	10.7 (0.3)

Crystallographic Study. A colorless crystal with dimensions 0.3 × 0.3 × 0.1 mm^3 of **11b** and a blue crystal with dimensions 0.2 × 0.2 × 1.0 mm^3 of **17a** were used for data collection at room temperature. The lattice parameters and intensity data were measured on a Philips PW-1100 automatic four-circle diffractometer by using graphite-monochromated Cu Kα radiation. Crystal data and data collection parameters are displayed in Table I. The structure was solved by the direct method for **11b** and the heavy-atom method for **17a** and refined by the block-diagonal-matrix least-squares method to R values of 0.061 and 0.066, respectively. The molecular structures are illustrated in Figures 2 and 3 by ORTEP drawings with 30% probability thermal ellipsoids. The atomic positional parameters are given together with their standard deviations in Tables II and III. Selected interatomic distances, short intramolecular hydrogen-bonded distances, and bond angles are presented in Tables IV–VI.

Phenol-Pendant Macrocyclic Tetraamines: 11a–c. The phenol-pendant 13-, 14-, and 15-membered macrocyclic monooxo tetraamines **10a–c** were synthesized by refluxing coumarin (**9**) and the linear tetraamines

Table IV. Bond Distances (Å) for **11b**, **17a**$(ClO_4)\cdot H_2O$, and **17b** with Estimated Standard Deviations in Parentheses

	free ligand **11a**	Cu^{II} complex **17a**$(ClO_4)\cdot H_2O$	Ni^{II} complex[a] **17b**
N(1)–C(2)	1.460 (4)	1.482 (7)	1.487 (8)
N(1)–C(14)	1.471 (4)	1.493 (8)	1.473 (10)
C(2)–C(3)	1.524 (5)	1.507 (8)	1.524 (11)
C(3)–N(4)	1.474 (3)	1.485 (7)	1.495 (11)
N(4)–C(5)	1.480 (4)	1.488 (7)	1.491 (9)
C(5)–C(6)	1.541 (4)	1.548 (8)	1.540 (11)
C(5)–C(15)	1.520 (4)	1.528 (7)	1.536 (11)
C(6)–C(7)	1.529 (5)	1.518 (8)	1.508 (9)
C(7)–N(8)	1.465 (4)	1.471 (8)	1.485 (10)
N(8)–C(9)	1.467 (4)	1.473 (10)	1.471 (9)
C(9)–C(10)	1.519 (5)	1.254 (15)	1.521 (12)
C(10)–N(11)	1.470 (4)	1.479 (13)	1.502 (12)
N(11)–C(12)	1.462 (4)	1.460 (8)	1.480 (10)
C(12)–C(13)	1.527 (5)	1.515 (10)	1.526 (14)
C(13)–C(14)	1.523 (5)	1.513 (8)	1.515 (11)
C(15)–C(16)	1.403 (4)	1.426 (7)	1.387 (9)
C(15)–C(20)	1.385 (4)	1.385 (7)	1.392 (10)
C(16)–C(17)	1.390 (5)	1.420 (8)	1.434 (12)
C(16)–O(21)	1.367 (3)	1.301 (6)	1.339 (9)
C(17)–C(18)	1.380 (5)	1.363 (8)	1.371 (13)
C(18)–C(19)	1.385 (5)	1.381 (8)	1.373 (12)
C(19)–C(20)	1.387 (5)	1.386 (8)	1.393 (12)
M–N(1)		2.035 (4)	2.072 (6)
M–N(4)		2.003 (4)	2.051 (5)
M–N(8)		2.037 (5)	2.085 (6)
M–N(11)		2.018 (5)	2.078 (5)
M–O(21)		2.145 (4)	2.015 (5)
M–O(1Cl)		3.135 (6)	2.402 (7)

[a] Here and in the following tables for **17b** data, crystal data and final fractional coordinates are found in the supplementary material of ref 11.

Table V. Short Intermolecular Bond Distances (Å) for **11b** and **17a**$(ClO_4)\cdot H_2O$ with Estimated Standard Deviations in Parentheses[a]

free ligand **11b**		Cu^{II} complex **17a**$(ClO_4)\cdot H_2O$	
N(1)···HN(4)	2.614 (26)	O(21)···HO(W)	1.964 (68)
N(1)···HN(11)	2.212 (26)	O(W)···HN(11)	2.344 (88)
N(8)···HN(4)	2.269 (24)	O(1Cl)···HN(4)	2.472 (56)
N(8)···HN(11)	2.493 (28)	O(2Cl)···H′O(W)*	2.252 (86)
N(4)···HO(21)	2.163 (34)	O(2′Cl)···H′O(W)*	2.301 (83)

[a] Atoms marked with an asterisk are at $x, y + 1, z$; other atoms are at x, y, z.

2a–c, respectively, in MeOH. Reduction of the monooxo derivatives with B_2H_6 afforded **11a–c**. Typically, the synthetic procedure of **11b** is as follows. Refluxing **9** (10.0 g, 68 mmol) and 1,9-diamino-3,7-diazanonane (**2b**) (10.9 g, 68 mmol) in 1.5 L of dry MeOH for 2 weeks affords 7-(2-hydroxyphenyl)-1,4,8,11-tetraazatetradecan-5-one (**10b**) as its trihydrochloride salt in 20% yield (5.7 g, 13.7 mmol), after purification by silica gel column chromatography (eluant CH_2Cl_2–MeOH–28% aqueous NH_3, 100:5:1) and recrystallization from EtOH–HCl: mp 185 °C dec. IR (KBr): ν_{CO} = 1640 cm^{-1}. Reduction of **10b**·3HCl (5.7 g) with freshly distilled B_2H_6 in THF yielded 5-(2-hydroxyphenyl)-1,4,8,11-tetraazatetradecane (**11b**; 2.0 g, 6.8 mmol) as colorless crystals in 50% yield. The product was purified by recrystallization from CH_3CN. ^1H NMR ($CDCl_3$): δ 0–1.5 (m, 1 H), 1.5–2.1 (m, 4 H), 2.3–3.2 (m, 18 H), 3.7–4.0 (dd, 1 H), 6.6–7.2 (m, 4 H). ^{13}C NMR ($CDCl_3$): δ 157.8, 127.9, 127.8, 126.6, 118.6, 116.4, 66.7, 51.2, 50.9, 50.1, 49.6, 49.3, 49.2, 47.3, 36.3, 29.3. The other physical data for all of the new compounds are listed in Table VII.

Phenyl- and 2-Methoxyphenyl-Pendant Cyclam: 7e,f. Refluxing cinnamic acid ester derivatives **5** and the linear tetraamine **2b** in dry MeOH afforded the monoxo derivatives **6**. The cyclam derivatives **7** were synthesized by reduction of **6** with B_2H_6. Typically, the synthetic procedure of **7e** is as follows. Refluxing the cinnamic acid ethyl ester **5e** (10.0 g, 57 mmol) and **2b** (9.1 g, 57 mmol) in 1.5 L of dry MeOH for 3 weeks afforded 7-phenyl-1,4,8,11-tetraazatetradecan-5-one (**6e**) as colorless crystals in 30% yield (5.0 g, 17.2 mmol). The product was purified by recrystallization from CH_3CN. IR (KBr): ν_{CO} = 1640 cm^{-1}. ^1H NMR ($CDCl_3$): δ 1.1–2.4 (m, 3 H), 1.6–1.9 (m, 2 H), 2.4–3.0 (m, 12 H), 3.2–3.5 (m, 2 H), 3.7–4.0 (dd, 1 H), 7.0–7.3 (m, 5 H), 8.4–8.7 (m, 1 H). Reduction of **6e** (5.0 g) with freshly distilled B_2H_6 in THF yields the cyclam derivative **7e** as its tetrahydrochloride salt in 50% yield (2.4 g, 8.6 mmol). The product was purified by recrystallization from EtOH–HCl. ^1H NMR ($CDCl_3$, as free form): δ 1.6–2.0 (m, 4 H), 2.2–3.0 (m, 18 H), 3.6–3.8 (dd, 1 H), 7.0–7.3 (m, 5 H). 7-(2-Methoxyphenyl)-1,4,8,11-tetraazacyclotetradecan-5-one (**6f**): IR (KBr) ν_{CO} = 1640 cm^{-1}; ^1H NMR ($CDCl_3$) δ 1.1–2.4 (m, 3 H), 1.6–1.9 (m, 2 H), 2.4–3.0 (m, 12 H), 3.2–3.6 (m, 2 H), 3.8 (s, 3 H), 3.9–4.1 (dd, 1 H), 6.6–7.1 (m, 4 H), 8.8–9.1 (m, 1 H). 5-(2-Methoxyphenyl)-1,4,8,11-tetraazacyclotetradecane (**7f**): ^1H NMR ($CDCl_3$) δ 1.5–2.0 (m, 4 H), 2.0–3.0 (m, 18 H), 3.75 (s, 3 H), 3.9–4.1 (dd, 1 H), 6.6–7.1 (m, 4 H).

5-(2-Hydroxy-5-nitrophenyl)-1,4,8,11-tetraazatetradecane (13). Refluxing 6-nitrocoumarin (**12**; 5.0 g, 26.2 mmol) and **2b** (4.2 g, 26.2 mmol) in 500 mL of dry MeOH for 3 days afforded 7-(2-hydroxy-5-nitrophenyl)-1,4,8,11-tetraazacyclotetradecan-5-one as its trihydrochloride salt in 19% yield (2.3 g, 5.0 mmol), after purification by silica gel column chromatography (eluant CH_2Cl_2–MeOH–28% aqueous NH_3, 1000:80:0.5) and recrystallization from EtOH–HCl: mp 195 °C dec. IR (KBr): ν_{CO} = 1630 cm^{-1}. ^1H NMR ($CDCl_3$ and CD_3OD, as free form): δ 2.0–2.3 (m, 2 H), 2.4–3.5 (m, 12 H), 3.7–4.0 (m, 1 H), 4.5–4.8 (dd, 2 H), 7.0–7.2 (d, 1 H), 8.0–8.4 (m, 2 H). Reduction of the monoamide compound (1.0 g, 2.85 mmol) with freshly distilled B_2H_6 in THF yielded the cyclam derivative **13** in 50% yield (480 mg, 1.42 mmol) as yellow

Table VI. Bond Angles (deg) for **11b**, **17a**$(ClO_4)\cdot H_2O$, and **17b** with Estimated Standard Deviations in Parentheses

	free ligand **11b**	Cu^{II} complex **17a**$(ClO_4)\cdot H_2O$	Ni^{II} complex **17b**
C(2)–N(1)–C(14)	112.6 (2)	114.0 (4)	114.1 (6)
C(3)–C(2)–N(1)	110.5 (2)	108.7 (4)	108.9 (6)
N(4)–C(3)–C(2)	110.0 (2)	107.9 (4)	107.6 (6)
C(5)–N(4)–C(3)	114.0 (2)	114.6 (4)	114.5 (5)
C(6)–C(5)–N(4)	110.6 (2)	108.6 (4)	109.6 (6)
C(6)–C(5)–C(15)	110.3 (2)	112.9 (4)	112.2 (6)
C(7)–C(6)–C(5)	115.9 (3)	116.6 (5)	116.7 (6)
N(8)–C(7)–C(6)	111.3 (3)	111.7 (5)	113.4 (6)
C(9)–N(8)–C(7)	113.2 (2)	113.9 (5)	114.6 (6)
C(10)–C(9)–N(8)	109.8 (3)	120.7 (9)	110.1 (7)
N(11)–C(10)–C(9)	109.2 (3)	119.6 (10)	107.2 (7)
C(12)–N(11)–C(10)	113.2 (2)	110.7 (6)	111.2 (6)
C(13)–C(12)–N(11)	111.0 (3)	112.2 (5)	111.6 (7)
C(14)–C(13)–C(12)	114.4 (3)	114.8 (5)	114.5 (7)
N(1)–C(14)–C(13)	111.8 (2)	112.4 (5)	111.8 (7)
C(16)–C(15)–C(5)	121.6 (2)	123.8 (4)	123.6 (6)
C(16)–C(15)–C(20)	117.8 (3)	119.7 (5)	120.6 (7)
C(5)–C(15)–C(20)	120.6 (2)	116.5 (4)	115.5 (6)
C(17)–C(16)–C(15)	120.8 (3)	116.2 (5)	117.2 (7)
C(17)–C(16)–O(21)	118.9 (3)	120.1 (5)	117.2 (6)
C(15)–C(16)–O(21)	120.2 (3)	123.7 (5)	125.6 (7)
C(18)–C(17)–C(16)	119.6 (3)	122.4 (5)	120.9 (8)
C(20)–C(19)–C(18)	118.9 (3)	118.1 (5)	118.8 (8)
N(1)–M–N(4)		86.0 (2)	85.6 (2)
N(1)–M–N(11)		93.3 (2)	92.7 (2)
N(4)–M–N(8)		94.3 (2)	96.6 (2)
N(8)–M–N(11)		85.5 (2)	84.9 (2)
N(4)–M–O(21)		87.5 (2)	88.8 (2)
N(8)–M–O(21)		98.0 (2)	94.1 (2)
O(21)–M–O(1Cl)		156.7 (2)	177.6 (2)
M–O(21)–C(16)		127.4 (3)	126.9 (4)

Table VII. Various Properties and Yields for New Macrocylic Polyamines

macrocyclic polyamine	mp, °C	M^+ peak, m/e (M_r)	anal. (C, H, N)[a]	yield, %
6e	155–157	290 (290.42)	$C_{16}H_{26}N_4O$	30[b]
6f	151–152	320 (320.44)	$C_{17}H_{28}N_4O_2$	25[b]
7e	266 dec	276 (276.43)[f]	$C_{16}H_{28}N_4\cdot 4HCl$	50[c]
7f	112–114	306 (306.46)	$C_{17}H_{30}N_4O$	60[c]
11a	72–74	278 (278.40)	$C_{15}H_{26}N_4O\cdot H_2O$	10,[b] 50[c]
11b	142–143	292 (292.43)	$C_{16}H_{28}N_4O$	20,[b] 50[c]
11c	256 dec		$C_{17}H_{30}N_4O\cdot 4HCl\cdot H_2O$	11,[b] 61[c]
13	215 dec		$C_{16}H_{27}N_5O_3\cdot HClO_4$	19,[b] 50[c]
15	234 dec		$C_{16}H_{25}N_6O_5\cdot HClO_4\cdot 0.5H_2O$	36,[d] 67[e]

[a] Compounds gave satisfactory analyses (±0.4%). [b] Cyclization yield. [c] Reduction yield. [d] Dinitration yield. [e] Deprotection yield. [f] Free form as colorless powder (by neutralization with 28% aqueous NH_3).

crystals of the monoperchlorate salt, recrystallized from water adjusted at pH 7 in the presence of excess sodium perchlorate. ^{1}H NMR (D_2O, NaOD): δ 1.5–2.9 (m, 2 H), 2.1–2.9 (m, 14 H), 4.0–4.2 (dd, 1 H), 6.3–6.4 (d, 1 H), 7.7–8.0 (m, 2 H).

5-(3,5-Dinitro-2-hydroxyphenyl)-1,4,8,11-tetraazacyclotetradecane (15). **11b** in 35 mL of trifluoroacetic anhydride was stirred at room temperature for 5 h, and then the solvent was evaporated in vacuo. The oily residue was dissolved in dichloromethane and the solution washed with water, dried, and evaporated in vacuo. Addition of diethyl ether afforded 1,4,8,11-tetrakis(trifluoroacetyl)-5-(2-hydroxyphenyl)-1,4,8,11-tetraazacyclotetradecane (**14**) in 94% yield (1.14 g, 1.7 mmol): mp 184–187 °C. IR (KBr): ν_{CO} = 1685 cm^{-1}. ^{1}H NMR ($CDCl_3$, $(CD_3)_2SO$): δ 1.7–2.4 (m, 4 H), 2.7–4.4 (m, 15 H), 6.6–6.9 (d, 2 H), 6.9–7.2 (d, 2 H). A mixture of 70% nitric acid (4.7 mL) with **14** (760 mg, 1.12 mmol) in 2.8 mL of 98% sulfuric acid was stirred at room temperature for 3 h and then poured into crushed ice and water to precipitate yellow crystals, which were collected by filtration. Recrystallization from methanol and diethyl ether afforded 1,4,8,11-tetrakis-(trifluoroacetyl)-5-(3,5-dinitro-2-hydroxyphenyl)-1,4,8,11-tetracyclotetradecane in 36% yield (310 mg, 0.4 mmol): mp 222–224 °C. IR (KBr): ν_{CO} = 1685 cm^{-1}. ^{1}H NMR ($CDCl_3$, CD_3OD): δ 1.6–2.4 (m, 4 H), 2.9–4.0 (m, 14 H), 4.0–4.2 (m, 1 H), 8.7–9.0 (m, 2 H). The dinitro derivative (310 mg, 0.40 mmol) was treated with 1 M NaOH solution (2.4 mL) in 10 mL of methanol, at room temperature for 20 h. The solvent was evaporated in vacuo, and 1 M perchloric acid was added (3.3 mL) to precipitate yellow crystals, which were collected by filtration. Recrystallization from water adjusted at pH 7 by 1 M NaOH solution afforded **15** (130 mg, 0.27 mmol) in 67% yield. ^{1}H NMR (D_2O, NaOD): δ 1.6–2.0 (m, 4 H), 2.3–3.0 (m, 14 H), 4.0–4.3 (dd, 1 H), 7.9 (d, 1 H), 8.5 (d, 1 H).

Preparation of the Copper(II) Complex with 11b: $[Cu^{II}(11b\cdot H_{-1})]ClO_4\cdot H_2O$ (17a(ClO_4)·H_2O). The phenol-pendant cyclam **11b** (146 mg, 0.5 mmol) and $CuSO_4\cdot 5H_2O$ (125 mg, 0.5 mmol) were dissolved in 50 mL of 0.5 M $NaClO_4$ aqueous solution at ca. 50 °C, and the mixture was adjusted to pH 8 with 0.1 M NaOH solution. The resulting blue solution was filtered, and the filtrate stood for 2 weeks at room temperature. Blue crystals of **17a** were obtained in ca. 50% yield (120 mg). Anal. Calcd for $C_{16}H_{27}N_4OCuClO_4\cdot H_2O$: C, 40.68; H, 6.19; N, 11.86. Found: C, 40.42; H, 6.18; N, 11.76.

Results and Discussion

Synthesis. Earlier, we reported the synthesis of the 14-membered monooxo tetraamine **3b** by condensation of ethyl acrylate (**1**) with 1,9-diamino-3,7-diazanonane (**2b**).[17] We have applied

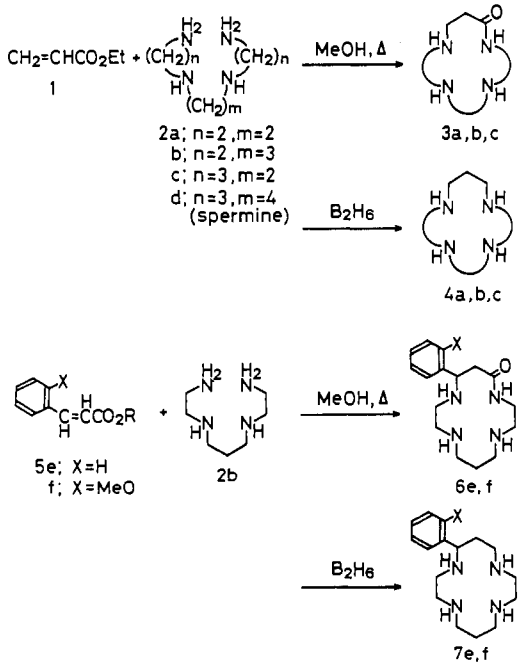

this annelation procedure to the synthesis of the phenyl-side-armed N_4 compounds **6** and **7** starting from phenyl-substituted α,β-unsaturated ester **5** and **2b**. Since **6e** happened to be a homologue of macrocyclic spermine alkaloids such as verbascenine (**8**),[18] an attempt was made to synthesize **6d** by substituting **2b** for spermine (**2d**) but almost no cyclization reaction occurred.

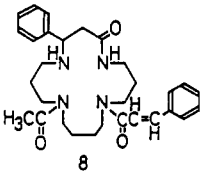

We have further extended this one-pot cyclization method to preparation of the phenol-side-armed macrocyclic N_4 compound **10**. The treatment of coumarin (**9**) with **2a–c** in refluxing dry

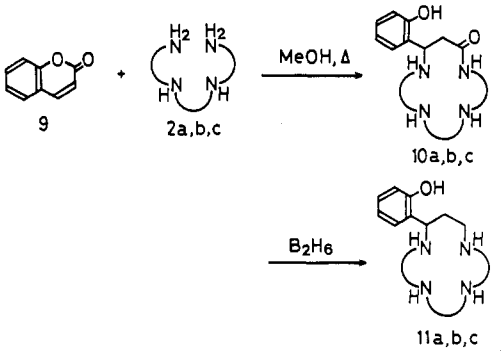

MeOH gave the corresponding 13- (**10a**), 14- (**10b**), and 15-membered (**10c**) monooxo N_4 compounds, respectively. Obviously, the annelation involves the reactions of the two terminal amines for the initial Michael type addition followed by an intramolecular lactamization. However, the annelation with spermine (**2d**) failed. The reduction of the lactam function was successful with diborane in tetrahydrofuran, leading to **11**.

The *p*-nitrophenol-pendant cyclam **13** was synthesized from 6-nitrocoumarin (**12**). The 2,4-dinitrophenol-pendant cyclam **15** was derived from nitration of the phenol-pendant tetrakis(trifluoroacetyl)cyclam **14** in HNO_3–H_2SO_4, followed by alkaline removal of the trifluoroacetyl groups.

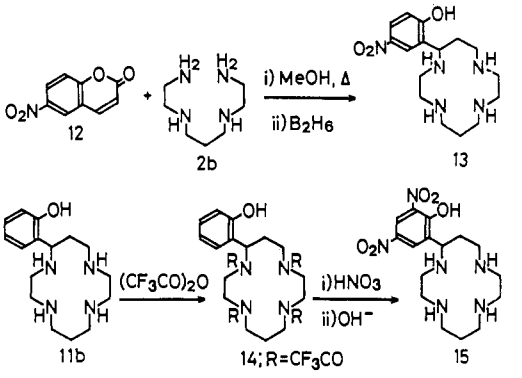

The present new synthetic method is also applicable to preparation of macrocyclic triamines[14] and pentaamines.[19] The pyridyl-pendant cyclam was prepared in a similar treatment of 3-(2-pyridyl)acrylic acid methyl ester with **2b**.[20] Since cyclic spermine and spermidine alkaloids often possess biological activities,[21] our macrocyclic polyamines may serve as good candidates for new drug design.

Ligand Properties. In $CHCl_3$ solution, the motion of the phenolic group of **11b** is restricted with its OH group strongly hydrogen bonded with the nearest nitrogen N(4) of the macrocycle (see X-ray structure of Figure 2). The ^{1}H NMR spectrum in

(17) Kimura, E.; Koike, T.; Machida, R.; Nagai, R.; Kodama, M. *Inorg. Chem.* **1984**, *23*, 4181–4188.

(18) (a) Seifert, K.; Johne, S.; Hesse, M. *Helv. Chim. Acta* **1982**, *65*, 2540–2547. (b) Guggisberg, A.; Hesse, M. *The Alkaloids*; Brossi, A., Ed.; Academic: New York, 1983; Vol. XXII, pp 85–188.

(19) Kimura, E., unpublished results.

(20) Kimura, E.; Koike, T.; Nada, H.; Iitaka, Y. *J. Chem. Soc., Chem. Commun.* **1986**, 1322–1323.

(21) Smith, T. A.; Negrel, J.; Bird, C. R. *Advances in Polyamine Research*; Bachrach, U., Kaye, A., Chayen, R., Eds.; Raven: New York, 1983; Vol. 4, pp 347–370.

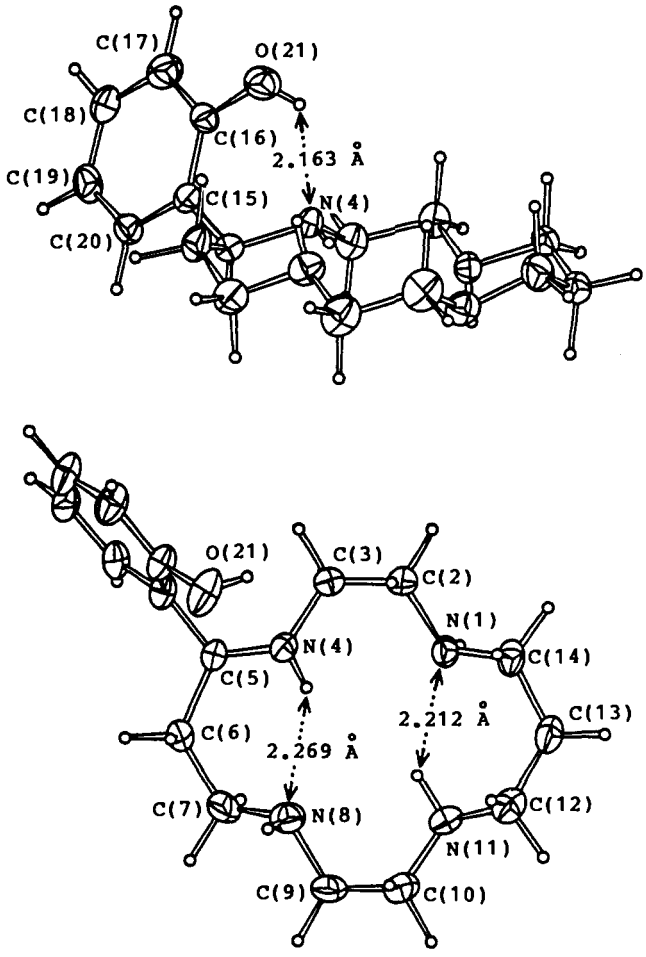

Figure 2. ORTEP drawings of **11b**: side-on view and top view. Atoms are drawn with 30% probability ellipsoids.

$CDCl_3$ at 35 °C shows an unusually high chemical shift for OH (0–1.5 ppm) and a well-resolved AB quartet for the benzylic H signal (3.82 ppm; J_A = 9.8 Hz, J_B = 3.4 Hz) owing to coupling with the adjacent CH_2 protons.

The most revealing property of phenols is their ionization in aqueous solution. The question arises, therefore, as to how the adjacent aza crown environment might affect the acidity of the phenols. The deprotonation constants (Table VIII) for new macrocycles were determined by pH-metric titrations aided by spectroscopic titrations (Figure 1 for **11b**). The deprotonation mode for **11b** is depicted as

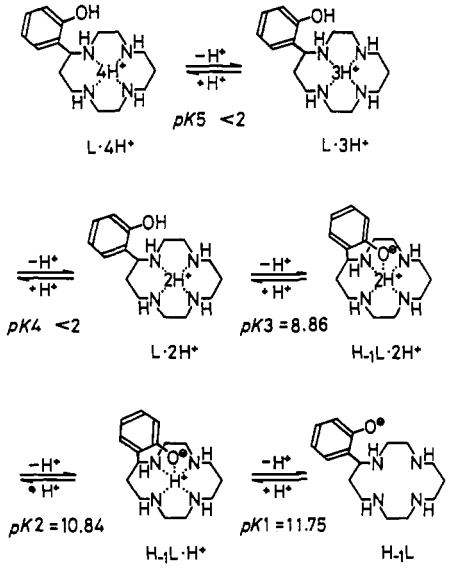

Table VIII. pK_a Values[a] and UV Data at I = 0.1 M ($NaClO_4$) and 25 °C

ligand	pK_a phenol	pK_a amines	UV abs max, nm (ε) phenol form	UV abs max, nm (ε) phenolate form
11a	8.71	11.54 10.31 <2 <2	272 (2300) [pH 4.0]	292 (3800) [pH 11.1]
11b	8.86	11.75 10.84 <2 <2	272 (2400) [pH 6.3]	292 (4000) [pH 11.3]
11c	8.76	11.74 10.21 4.77 3.34	272 (2300) [pH 7.0]	292 (3800) [pH 11.0]
phenol	10.0		269	287
4b(cyclam)[b]		11.50 10.20 ca. 1.7 ca. 1.0		
13	6.37	11.78 10.44 <2 <2	320 (9800) [pH 3.6]	403 (17 400) [pH 9.6]
p-nitrophenol	7.1		317	400
15	2.90[c]		264 (13 300) [pH 1.6]	367 (16 200) [pH 5.8]
2,4-dinitrophenol	4.1		260	360

[a] Determined potentiometrically unless otherwise noted. [b] Kodama, M.; Kimura, E. *J. Chem. Soc., Dalton Trans.* **1976**, 1721–1724. [c] Determined spectrophotometrically at [**15**] = 0.1 mM.

The pK_a value of 8.86 (**11b**) at 25 °C and I = 0.1 M ($NaClO_4$) is smaller than the pK_a value of 10.0 for phenol itself, evidently due to the proximate dipositive charge of the N_4 aza crowns. The UV absorption maxima (Table VIII) for the phenol and phenolate forms discretely occur at 272 and 292 nm, respectively, with isobestic points at 257 and 278 nm. The variation of the N_4 ring size does not significantly affect the pK_a value of the phenol. Existence of the adjacent phenolate anion raises the basicity of the macrocyclic polyamines (cf. the deprotonation constants for K_1 and K_2 with or without the phenol pendant). The phenolate basicities (in H_2O) of **13** (pK_a 6.37) and **15** (pK_a 2.90) were also decreased by the adjacent diprotonated cyclams.

Interestingly, the N_4-diprotonated species $(H_{-1}L{\cdot}2H^+)^+$ (L = **11b**, **13**, and **15**) are isolable as crystalline monoperchlorate salts out of pH 9.5, 7.0, and 7.0 aqueous solutions, respectively, in the presence of an excess amount of $NaClO_4$. The zwitterionic structure is demonstrated by their UV spectra (in H_2O) of the phenolate forms. In nonaqueous MeOH or $CHCl_3$ solution, the phenol hydrogen of **11b** remains undissociated as shown by the UV spectral measurement (λ_{max} 278 nm, ε 2300).

Crystal Structure of the Free-Ligand Phenol-Pendant Cyclam 11b. The structure of **11b** is shown in Figure 2. Selected molecular dimensions, bond distances, short hydrogen bond distances, and torsion angles are in Tables II, IV, V, and IV, respectively. The N_4 macrocyclic (cyclam) conformation is similar to those reported for Cu^{II}–[22] and Ni^{II}–cyclam[23] complexes, except that N(4)–H and N(11)–H bonds lie approximately in the N_4 plane. The macrocycle conformation is stabilized by the two hydrogen bonds N(4)H···N(8) = 2.269 (24) Å and N(11)H···N(1) = 2.212 (26) Å. The phenol ring is oriented vertically to achieve the intramolecular hydrogen bond with the nearest ring nitrogen N(4), O(21)H···N(4) = 2.163 (34) Å. This solid configuration of crystals accounts well for the above-mentioned ^1H NMR signal of the doublet of doublets for the benzylic H.

(22) Tasker, P. A.; Sklar, L. *J. Cryst. Mol. Struct.* **1975**, *5*, 329.
(23) Bosnich, B.; Mason, R.; Pauling, P. J.; Robertson, G. B.; Tobe, M. L. *J. Chem. Soc., Chem. Commun.* **1965**, 97–98.

Table IX. Effects of the Concentration of L (**11b**) and pH on the Half-Wave Potentials at I = 0.20 M ($NaClO_4$) and 25 °C

(a) Concentration Effect: [Cu^{II}] = 0.15 mM, pH 10.30 (0.02 M Borate)

[**11b**], mM	$E_{1/2}$, V vs. SCE	$\Delta E_{1/2}$, mV calcd[a]	$\Delta E_{1/2}$, mV obsd
1.50	−0.7785	0	0
2.00	−0.7822	−3.7	−3.7
3.00	−0.7875	−8.9	−9.0

(b) pH Effect: [Cu^{II}] = 0.20 mM, [**11b**] = 2.00 mM, [Borate] = 0.02 M

pH	log [$A(H^+)$]	$E_{1/2}$, V vs. SCE	$\Delta E_{1/2}$, mV calcd[a]	$\Delta E_{1/2}$, mV obsd
10.30	2.131	−0.7822	+57.0	+55.6
10.80	1.307	−0.8092	+32.6	+28.4
11.37	0.617	−0.8276	+12.3	+10.2
12.01	0.201	−0.8378	0	0

[a] From eq 1.

Complex Formation of 11b with M^{II}. In aqueous solutions, Cu^{II}, Ni^{II}, and Fe^{II} all form the apical phenolate-coordinating complexes $M^{II}H_{-1}L$ (**17**). The first two complexes $Cu^{II}H_{-1}L$ (**17a**) and

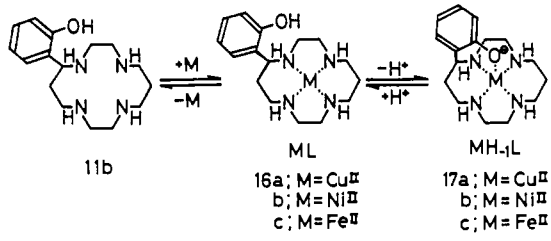

$Ni^{II}H_{-1}L$ (**17b**) were isolated as monoperchlorate salts out of pH 11 solutions to be subjected to X-ray crystal analysis. An attempt to isolate $Fe^{II}H_{-1}L$ (**17c**) failed. The crystal structure of the Ni^{II} complex **17b** was communicated earlier.[11] Its detailed structure parameters are listed in comparison with those of the Cu^{II} counterpart **17a** in Tables IV–VI.

The $Fe^{II}H_{-1}L$ (**17c**) formation was shown by the pH-metric titration of **11b** in the presence of 1 equiv of $FeSO_4$ under an argon atmosphere (Figure 1b), which indicates the simultaneous N_4 and phenol dissociation below neutral pH (see smooth buffer region until a = 5). The occurrence of phenol dissociation far below the pK_a value of the free ligand suggests the strong tendency of phenolate coordination to help capture Fe^{II} in the N_4 macrocycle. On the basis of the titration behavior we assign the Fe^{II} complex structure **17c** similar to those of Ni^{II} and Cu^{II} complexes. From the analysis of the titration data (indicated as × in Figure 1b), the 1:1 complexation constant $K_{Fe^{II}H_{-1}L}$ (=[$Fe^{II}H_{-1}L$]/[Fe^{II}][$H_{-1}L$]) of 6.3 × 10^{14} at 25 °C and I = 0.1 ($NaClO_4$) was determined. The theoretical curve based on the obtained parameters (Figure 1b) accommodates well the experimental data. The yellow Fe^{II} complex **17c** in aqueous solution (λ_{max} 455 nm, ϵ 200 at pH 7.4) is high spin (μ_{eff} = 5.19 μ_B at 35 °C by the Evans method[24]) and is oxidized immediately in air to the Fe^{III} complex. We presume the fundamentally same complex configuration is retained with Fe^{III}. It is to be added that the Fe^{II} complexes of cyclam without the phenol (e.g. cyclam and **7**) exist only in nonaqueous solutions and are very rapidly oxidized to Fe^{III} oxide precipitates in water.[25]

With Cu^{II}, the pH titration curve (Figure 1c) suggests a stepwise complexation manner, initially to $Cu^{II}L$ (**16a**) and then to $Cu^{II}H_{-1}L$ (**17a**). Since the Cu^{II} the complexation buffer pH is too low to permit an accurate resolution, we have turned to the polarographic technique for the complexation constants.[26] In the alkaline pH region, Cu^{II} ion in the presence of excess ligand **11b** produces a reversible, 2e reduction polarogram for $(Cu^{II}H_{-1}L)^+ + 2e^- + Hg \rightleftharpoons Cu(Hg) + H_{-1}L$. Its half-wave potential $E_{1/2}$ at ca. −0.8 V vs. SCE shifts with variation of pH and the ligand concentration in agreement with theoretical eq 1 (see Table IX),

$$E_{1/2} = E_{1/2}(Cu^{II}) - E_{1/2}(Cu^{II}H_{-1}L)$$
$$= 0.0296 \log (K_{CuH_{-1}L}[L]_f/A(H^+)) + \text{constant} \quad (1)$$

where $[L]_f$ is the concentration of the uncomplexed ligand and $A(H^+) = 1 + (a_{H^+})/K_1 + (a_{H^+})^2/K_1K_2 + ... + (a_{H^+})^5/K_1K_2K_3K_4K_5$.

Hence, $K_{CuH_{-1}L}$ (=[$Cu^{II}H_{-1}L^+$]/[Cu^{II}][$H_{-1}L^-$]) = 1.0 × 10^{32} M^{-1} at 25 °C and I = 0.20 M ($NaClO_4$) was determined from eq 1. Table IX includes the calculated ($E_{1/2}$) values derived from eq 1 and $K_{CuH_{-1}L}$, which show good agreement with the experimental values. For the phenolate protonation process $CuH_{-1}L^+ + H^+ \rightleftharpoons CuL^{2+}$ (at $4 < a < 5$, see Figure 1c), the pK_a value of 9.15 and ligand K_1 value were used to calculate K_{CuL} (=[$Cu^{II}L^{2+}$]/[Cu^{II}][L]) of 2.5 × 10^{29} M^{-1}. The comparison of K_{CuL} and $K_{CuH_{-1}L}$ values discloses 400 times stability enhancement by the intramolecular phenolate coordination.

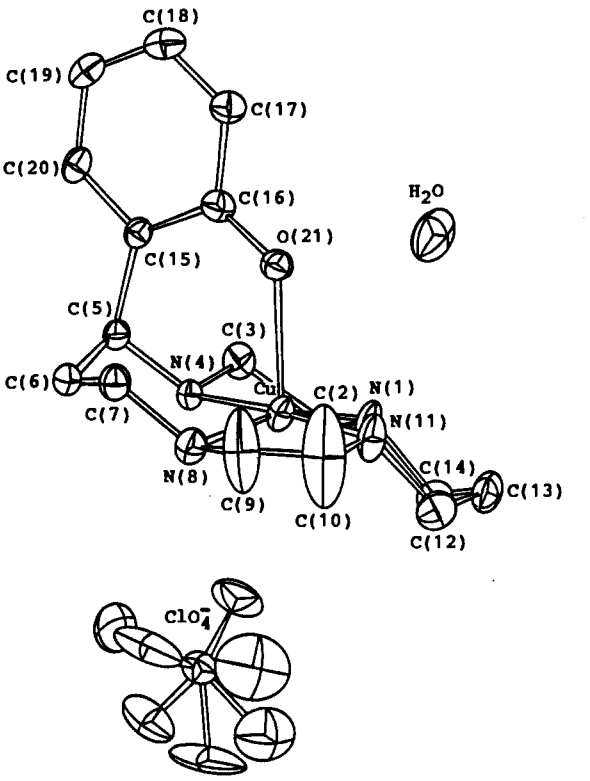

Figure 3. ORTEP drawing of complex **17a**(ClO_4)·H_2O. Atoms are drawn with 30% probability ellipsoids. Hydrogen atoms are omitted for clarity.

Crystal Structure of [Cu^{II}(phenol-pendant cyclam)]ClO_4·H_2O (17a(ClO_4)·H_2O). The side view is shown in Figure 3. The bond parameters are listed in comparison with those for free ligand **11b** and its Ni^{II} complex[11] in Tables IV–VI. The configurations of the macrocyclic ligand are fundamentally identical for Cu^{II} and high-spin Ni^{II} complexes **17**. An ideal position of the phenol for the apical coordination to Cu^{II} is evident. The basal cyclam N_4

(24) Evans, D. F. *J. Chem. Soc.* **1959**, 2003–2005.
(25) Watkins, D. D., Jr.; Riley, D. P.; Stone, J. A.; Busch, D. H. *Inorg. Chem.* **1976**, *15*, 387–393.

(26) The polarograms of the Cu^{II}–cyclam complex exhibited two irreversible reduction waves *in the acidic pH region*, and hence we resorted to a potentiometric method to seek the stability constant of $10^{27.2}$, which is apparently a mean value for two isomeric complexes (Kodama, M.; Kimura, E. *J. Chem. Soc., Dalton Trans.* **1977**, 1473–1478). In this work, we have discovered that both Cu^{II}–cyclam and Cu^{II}–phenol-pendant cyclam complexes show only one reversible 2e-reduction wave *in the alkaline pH >10 region.* The reversibilities are checked by plots of log [$i/(i_d - i)$] against the dc potential being invariably linear with a reciprocal slope of 30 mV (corresponding to a reversible two-electron reduction) at 25 °C. Therefore, we have determined the stability constants by the polarographic method. The present stability constant of the Cu^{II}–cyclam complex is $10^{30.5}$, which is almost the same as $10^{29.4}$ for the protonated phenol-pendant cyclam complex.

Table X. Visible and UV Absorption Spectra (at 25 °C, I = 0.1) and ESR Parameters (at 77 K) of Phenol-Pendant Macrocyclic Tetraamine (N_4) Complexes with Cu^{II}

ligand	phenol form	visible λ_{max}, nm (ϵ)	UV λ_{max}, nm (ϵ)	ESR $g_\perp$	ESR $g_\parallel$	ESR $A_\parallel$, G
13-membered **11a**	$-O^-$	572 (200) [pH 10.1]	238 (12200), 290 (sh, 4900) [pH 10.6]	2.05	2.19	190
	-OH	501 (180) [pH 3.6]	264 (6200) [pH 4.5]	2.05	2.16	205
[13]aneN$_4$		546[a]		2.05	2.18	184
14-membered **11b**	$-O^-$	557 (120) [pH 10.7]	238 (1500), 280 (sh, 5500) [pH 10.7]	2.06	2.20	200
	-OH	510 (70) [pH 6.5]	260 (8000) [pH 6.5]	2.05	2.19	205
[14]aneN$_4$ (cyclam)		503[a]		2.05	2.19	205[b]
15-membered **11c**	$-O^-$	742 (220) [pH 9.5]	236 (12800), 283 (8900) [pH 10.1]	2.06	2.21	155
	-OH	582 (160) [pH 4.3]	273 (10400) [pH 4.7]	2.06	2.21	183
[15]aneN$_4$		568[a]				

[a] Fabbrizzi, L.; Micheloni, M.; Paoletti, P. *J. Chem. Soc., Dalton Trans.* **1979**, 1581–1584. [b] Miyoshi, K.; Tanaka, H.; Kimura, E.; Tsuboyama, S.; Murata, S.; Shimizu, H.; Ishizu, K. *Inorg. Chim. Acta* **1983**, *78*, 23–30.

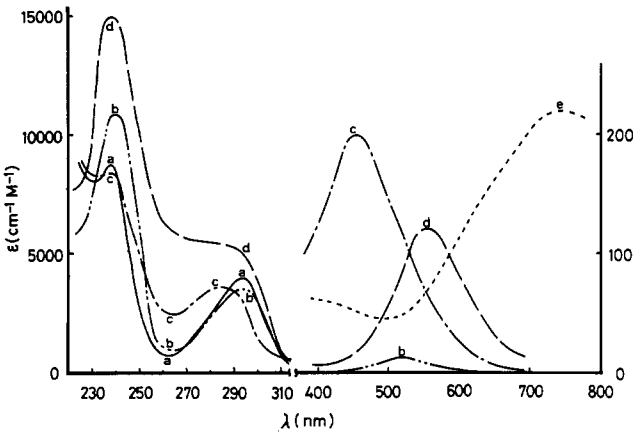

Figure 4. UV absorption spectra (λ_{max}, nm (ϵ); 25 °C; I = 0.1 M (NaClO$_4$)): (a) **11b** (292 (4000), 237 (8700)) at pH 11.3; (b) **17b** (520 (12), 293 (3700), 240 (11000)) at pH 8; (c) **17c** (455 (200), 284 (3800), 237 (8000)) at pH 7.4; (d) **17a** (557 (120), 238 (15000)) at pH 10.7; (e) **21a** (742 (220)) at pH 9.5.

retains the most stable trans-III configuration[3] with copper ion lying coplanar with N_4, as seen in tetragonally elongated *trans*-Cu(cyclam)(ClO$_4$)$_2$[22] and *trans*-Cu(cyclam)(SC$_6$F$_5$)$_2$.[27]

The four equatorial Cu–N bond lengths 2.035 (4), 2.003 (4), 2.037 (5), and 2.018 (5) Å are almost proportionally shorter than the corresponding high-spin Ni^{II}–N lengths in **17b**. Both metal ions are off the center of the N_4 cavity toward N(4) to come under the phenol O(21). The cyclam N atoms in **17a** tend to bind less strongly with Cu^{II} under the influence of the axial interaction with respect to those (at 2.01 Å) in tetragonally elongated Cu(cyclam)(ClO$_4$)$_2$[22] and Cu^{II}(cyclam)(SC$_6$F$_5$)$_2$.[27] An unusually large thermal motion of C(9) and C(10) (Figure 2), in conjunction with a very short C(9)–C(10) bond distance, suggests an unrigid conformation of the five-membered chelate involving these carbons.[28] The apical phenolate oxygen O(21) is slightly bent off the perpendicular to the Cu–N_4 plane so as to help elongation of the apical bond distance to 2.145 (4) Å, which is longer than the almost upright apical bond (2.015 Å) of the Ni^{II} counterpart.[11] The other apical Cu–O(1Cl) (of perchlorate) distance is extremely long at 3.135 (6) Å, indicating a virtually nonbonding interaction. Apparently, this is due to the trans effect of the Cu–phenolate compulsive interaction. In the six-coordinate, high-spin Ni^{II} complex **17b**, this apical bond length Ni–O (of perchlorate) is shorter, 2.402 Å. In the apically elongated, six-coordinate *trans*-Cu^{II}(cyclam)(ClO$_4$)$_2$, the Cu–O (of perchlorate) bond is 2.574 Å.[22]

Phenol–Phenolate Equilibrium in Metal Complexes. The ease of the apical phenol dissociation of cyclam derivatives (**16** ⇌ **17**) varies with the metal ions. In comparison with the dissociation constant pK_a of 8.86 for the diprotonated ligand L·2H$^+$ (L = **11b**), the Ni^{II} complex **16b** shows a much smaller value of 6.30, as determined by the pH-metric titration of 1 mM Ni^{II} complex **17b** with 0.1 M HClO$_4$ at 25 °C and I = 0.1 (NaClO$_4$), which indicates closer interaction for the Ni^{II} phenolate. With the Cu^{II} complex **16a**, it was similarly measured to be 9.15, evidence supporting an unfavorable axial ArO^-–Cu^{II} coordinate interaction. The closer interaction for ArO^-–Ni^{II} than for ArO^-–Cu^{II} is to be compared in terms of the bond lengths. The protonation constant of the Fe^{II} complex **16c** is estimated to be roughly 6.8 (see Figure 2b).

The N_4 macrocyclic ring size affects the phenol–phenolate equilibrium in Cu^{II} complexes. In the 13-membered homologous complex **18a**, the phenol dissociation is significantly easier (pK_a = 6.5, determined pH metrically and spectrophotometrically) than that of the 14-membered **16a**, suggesting a stronger ArO^-–Cu^{II} interaction in the smaller macrocyclic system. This may reflect the fact that the Cu^{II} ion is squeezed out of the smaller (coplanar) N_4 cavity to come closer to the apical phenolate, or one may envisage the folded 13-membered macrocyclic configuration **19** with the phenolate occupying a basal position. This is indeed the case with the high-spin Ni^{II} complex **19b**, as determined by an X-ray crystal structure study.[12] In the larger 15-membered N_4 macrocycle **20a** the pK_a is 7.8 (determined pH metrically), which is still lower than the value 9.2 for the 14-membered homologue. This is interpreted that the looser 15-membered ligand field (LF) does not cause elongation of the apical ArO^-–Cu bond as much as the tight 14-membered LF. With less strongly coordinating high-spin Ni^{II}, the ring size does not significantly influence pK_a values of the phenol and all are in a similar range: 6.7 for **18b** and 6.8 for **20b**.

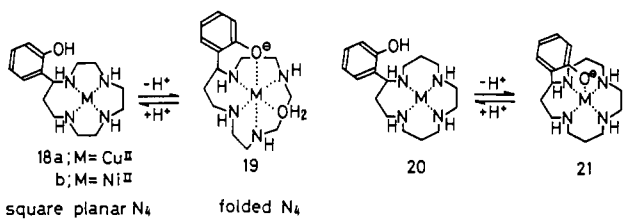

Effects of the Intramolecular Phenolate Coordination. Cu Complexes. The apical phenolate coordination to Cu^{II} in the 13–15-membered N_4 compounds **11a–c** significantly shifts their d–d transition bands to higher wavelengths (Table X; for 14-N_4 (**17a**) and 15-N_4 (**21a**), see Figure 4d,e). This is most remarkable with the largest 15-membered macrocycle **11c**. The N_4O LF strength of **17a** is almost equivalent to that of a 16-membered macrocyclic pentaamine (λ_{max} 560 nm).[29] The perturbed visible

(27) Addison, A. W.; Sinn, E. *Inorg. Chem.* **1983**, *22*, 1225–1228.
(28) In view of the abnormally short C(9)–C(10) bond length of 1.25 Å with thermal disorders at these carbon atoms, we have tried to refine them further, but with no further improvement. The elemental analysis for the complex and ^{1}H NMR analysis of the ligand removed from the complex (with H_2S and ion-exchange resin treatment) have confirmed that the ligand in the Cu^{II} complex is not dehydrogenated but is intact **11b**. These facts indicate that the shortened C(9)–C(10) bond of 1.25 Å is a shadow length resulting from thermal vibrations between two macrocyclic conformers.
(29) Kodama, M.; Kimura, E. *J. Chem. Soc., Dalton Trans.* **1978**, 104–110.

spectra in the region of the phenolate bands imply considerable orbital overlapping between phenolate and Cu. Upon its protonation to **16a**, the d–d bands become similar to those of the phenolate-free cyclam complexes. However, an interesting exception is seen with the 13-membered N_4 compound **11b**. From the occurrence of isosbestic points in the UV–visible spectra it was confirmed that protonation involves only the phenolate–phenol equilibrium in all of these complexes. The ESR parameters (at 77 K, see Table X) show the perturbation of the square-planar LF by the apical phenolate coordination. The distortion is most remarkable in 15-membered **21a**. The ESR parameters suggest the 13-membered N_4 complex structure becomes nearer to that of cyclam in the presence of pendant phenol (in protonated form); i.e. a well-fit square-planar N_4 LF is achieved in **18a**.

Fe Complexes. The compulsory intramolecular phenolate coordination makes saturated N_4 macrocycles a new type of sequestering agent for Fe^{III} in neutral aqueous solution. Cyclams without the phenol pendant (e.g. **7e**) cannot take up Fe^{III} nor dissolve $Fe(OH)_3$ in aqueous solution. The Fe^{II} complex **17c** shows a quasi-reversible (one-electron) cyclic voltammogram (CV), from which we determined the redox potential for $Fe^{III/II}$ as –0.16 V vs. SCE (at $7 < pH < 9$, nonbuffered, $I = 0.1$ ($NaClO_4$)). Mild air oxidation or electrochemical oxidation (at 0 V) of the yellow Fe^{II} complex solution yields the wine red Fe^{III} complex **17c**, which shows a CV identical with that obtained for the initial Fe^{II} complex. The same wine red Fe^{III} complex was directly prepared from **14b** and Fe^{III} (although its formation rate is much slower), which can be reduced again to the Fe^{II} complex with $Na_2S_2O_4$. On the basis of the reversible $Fe^{III/II}$ redox nature, we calculated a conditional constant $K'_{Fe^{III}H_{-1}L}$ ($=[Fe^{III}H_{-1}L]/[Fe^{III}][H_{-1}L]$) at pH 7.0 to be 4.0×10^{26} M^{-1}. Obviously, the phenolate coordination should contribute to stabilization of the Fe^{III} state with respect to the Fe^{II} state. Although another expression of the conditional stability constant K'' ($=[Fe^{III}H_{-1}L]/[Fe^{III}][\text{total uncomplexed L}]$) at pH 7.0 of 1.2×10^{16} M^{-1} is smaller than 5.0×10^{21} M^{-1} of Fe^{III}–EDTA,[30] the ligand-exchange reaction of Fe^{III} from **11b** to EDTA practically does not occur, owing to the kinetic inertness of macrocyclic ligand dissociation. Phenolate-free Fe complexes tend to have higher $Fe^{III/II}$ redox potentials (e.g. macrocyclic pentaamine complex –0.04 V,[31] hemoglobin –0.07 V at pH 7[32]). However, the value of –0.16 V is higher than those for Fe^{III} carriers such as mugineic acid (–0.34 V),[33] microbial hydroxamates (–0.59 to –0.69 V),[33] and enterobactin (–0.99 V).[34]

The electronic spectrum of the Fe^{III} complex **17c** is shown in Figure 4c. The visible band (480 nm) is assigned to the phenolate $\rightarrow Fe^{III}$ ($p\pi \rightarrow d\pi^*$) charge-transfer transition. Such $p\pi \rightarrow d\pi^*$ transitions are intense, whereas d–d transitions are very weak and are difficult to detect for Fe^{III}. Recently,[35] phenolate-to-Fe^{III} CT transitions in square-pyramidal Fe^{III}(salen)–OC_6H_4X complexes were studied, wherein the apical phenolate-to-Fe^{III} CT red-shifts as the phenolate ($-OC_6H_4X$) becomes more electron-donating. The decrease in this CT energy represents the increased binding of the phenolate ligands. This is also the case for our square-pyramidal $Fe^{III}N_4$–OC_6H_4X complexes: the *o*-methoxyphenolate-pendant cyclam complex exhibits the CT band at 518 nm (ϵ 2150).[36] It was also demonstrated that the stronger the basal salen ligand fields are, the higher the energy of the apical phenolate CT band.[34] The CT band of 480 nm with **17c** against that of 420 nm with the salen complex may suggest stronger apical Fe^{III}–phenolate bonding in the former than in the latter, in connection with the weaker basal ligand field in the former than in the latter.

Interestingly, our intense CT spectrum is similar to those of the Fe^{III}-transport serum protein transferrin, which shows λ_{max} 470 nm (ϵ 2500 for two Fe^{III} atoms binding),[37] and to lactoferrin, which shows λ_{max} 465 nm (ϵ 4140 for two Fe^{III} binding).[38] The high-spin Fe^{III}-binding sites in those proteins were mimicked by using small molecular ligands containing phenol(s).[35,39]

Upon acidification, the red Fe^{III} complex **16c** solution turned to purple (until absorption maximum λ_{max} 555 nm, ϵ 2300 at pH 4.3). We postulate dissociation of Fe^{III} out of the N_4 cavity by the protonations while there is still binding to the phenolate. The CT band of **16c** remained the same at higher pH (until ~10).

The nitro-substituted phenol cyclams **13** and **15** failed to sequester Fe ions in aqueous solution, and only Fe^{III} oxide precipitation resulted. This is due to insufficient electron donation by the effect of nitro group(s). With electron-donating substituents such as the *o*-methoxy group, Fe ions are more tightly bound than in the unsubstituted phenol cyclam **11b**.[10,19]

Ni Complexes. The strong apical coordination of the phenolate in **17b** (see the very short Ni–O bond distance; Table IV) should contribute to fix Ni^{II} in the pink high-spin state in the solid as well as in aqueous solution (λ_{max} 520 nm (ϵ 10) and $\mu_{eff} = 2.90$ μ_B by the Evans method[24] at 35 °C and $I = 0.1$ M ($NaClO_4$)). Upon protonation of the intramolecular apical phenolate to **16b** (at pH 3.5), Ni^{II} becomes a mixture of high spin and low spin with a lowered μ_{eff} value of 2.35 μ_B and appearance of a yellow band (λ_{max} 453 nm). The identical μ_{eff} value was reported earlier for the Ni^{II}–cyclam complex.[11]

The phenolate-pendant cyclam **17b** showed a significantly lowered redox potential, +0.35 V vs. SCE (0.5 M Na_2SO_4, pH 7.5, 25 °C), for $Ni^{III/II}$ with respect to that (+0.50 V vs. SCE under the same conditions; literature value +0.50 V[40]) of the Ni^{II}–cyclam complex. Namely, the higher oxidation state is stabilized with the apical phenolate ligand strength. Since addition of 10 times excess phenol to Ni^{II}–cyclam does not change the $Ni^{III/II}$ potential, it is concluded to be the effect of the intramolecularly bonded phenolate anion. Upon protonation of the coordinated phenolate ion below pH 6.5 the pendant phenol loses coordinating ability with Ni^{II} and the resulting complex **16b** exhibits a redox potential of +0.50 V vs. SCE (0.5 M Na_2SO_4, pH 5.2, 25 °C), the same value as for the Ni^{II}–cyclam complex. The UV spectrum of the crystalline **17b** in H_2O (Figure 4b) indicates phenolate bands at λ_{max} 293 nm (ϵ 3700) and 240 nm (ϵ 11 000), almost the same as for the uncoordinated phenolate anion (292 nm (ϵ 4000) and 237 nm (ϵ 8700)). These facts indicate little mixing between the nickel and phenolate orbitals or mostly an electrostatic nature of the apical bonding in **17b**.

The Ni^{III} complex **22** generated by oxidation of the Ni^{II} complex **17b** with $(NH_4)_2S_2O_8$ or by electrochemical oxidation at +0.5 V, pH 8, and 25 °C is not as stable as Ni^{III}–cyclam in solution and gradually decomposes through the Ni^{III} self-oxidation of the bound phenolate. The phenol alone (in free ligand **11b**) undergoes

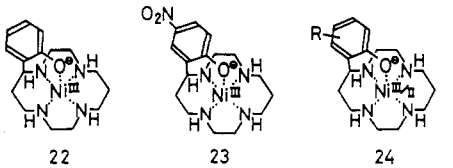

22 23 24

oxidation at ~+0.5 V (pH 10). On the other hand, the *p*-nitrophenolcyclam complex of Ni^{III} **23** is very stable. The freshly prepared Ni^{III} complex **22** shows a CV identical with that of the starting Ni^{II} complex **17b**. Its ESR spectrum in frozen aqueous

(30) Skochdopole, R.; Chaberek, S. *J. Inorg. Nucl. Chem.* **1959**, *11*, 222.
(31) Kimura, E.; Kodama, M.; Machida, R.; Ishizu, K. *Inorg. Chem.* **1982**, *21*, 595–602.
(32) Dryhurst, G.; Kadish, K. M.; Scheller, F.; Renneberg, R. *Biological Electrochemistry*; Academic: New York, 1982; Vol. I.
(33) Mino, Y.; Ishida, T.; Ota, N.; Inoue, M.; Nomoto, K.; Takemoto, T.; Tanaka, H.; Sugiura, Y. *J. Am. Chem. Soc.* **1983**, *105*, 4671–4676.
(34) Harris, W. R.; Carrano, C. J.; Raymond, K. N. *J. Am. Chem. Soc.* **1979**, *101*, 2722–2727.
(35) Heistand, R. H., II; Lauffer, R. B.; Fikrig, E.; Que, L., Jr. *J. Am. Chem. Soc.* **1982**, *104*, 2789–2796.
(36) Kimura, E.; Joko, S.; Koike, T.; Kodama, M., *J. Am. Chem. Soc.*, in press.
(37) Gaber, B. P.; Miskowski, V.; Spiro, T. G. *J. Am. Chem. Soc.* **1974**, *96*, 6868–6873.
(38) Ainscough, E. W.; Brodie, A. M.; Plowman, J. E.; Brown, K. L.; Addison, A. W.; Gainsford, A. R. *Inorg. Chem.* **1980**, *19*, 3655–3663.
(39) Pyrz, J. W.; Roe, A. L.; Stern, L. J.; Que, L., Jr. *J. Am. Chem. Soc.* **1985**, *107*, 614–620.
(40) Zeigerson, E.; Ginzburg, G.; Schwartz, N.; Luz, Z.; Meyerstein, D. *J. Chem. Soc., Chem. Commun.* **1979**, 241–243.

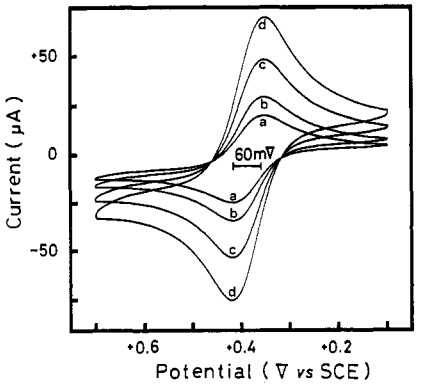

Figure 5. Cyclic voltammograms for the $Ni^{III/II}$–*p*-nitrophenol-pendant cyclam complex **23** at a glassy-carbon electrode at 25 °C, pH 7.0, and I = 1.5 M (Na_2SO_4). The scan rates (a–d) are 10, 20, 50, and 100 mV s^{-1}, respectively.

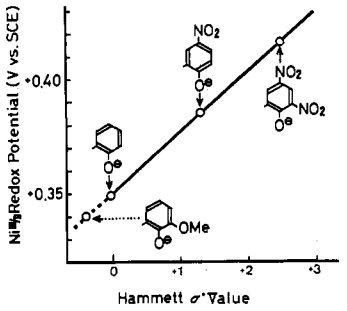

Figure 6. Plots of $Ni^{III/II}$ redox potential values for substituted-phenolate-pendant cyclam–Ni complexes against Hammett σ^* values.

solution at 77 K with $g_\perp$ = 2.18 and $g_\parallel$ = 2.03 is almost the same as that for Ni^{III}–cyclam.[40,41] The Ni^{III} complex **22** shows intense charge-transfer absorptions at λ_{max} 318 nm (ϵ 7000) and 290 nm (ϵ 9000), while the CT's for Ni^{III}–cyclam occur at λ_{max} 370 nm (sh, ϵ 6000) and 295 nm (ϵ 11 000).[40]

The redox potentials $E_{1/2}$ for $Ni^{III/II}$ in substituted-phenol cyclam complexes **24**, which were determined by cyclic voltammetry, vary with substituents R. A typical CV with R = *p*-nitro is shown in Figure 5, which demonstrates well neat reversible redox behaviors. An electron-withdrawing R tends to increase the oxidation potential. Plots of $E_{1/2}$ vs. Hammett σ^* values[42] (Figure 6) are linear. Very interestingly, when R becomes *o*-methoxy (σ^* = −0.39), the $E_{1/2}$ value (of +0.34 V) for $Ni^{III/II}$ is anticipated to coincide with the 2e oxidation potential (+0.30 V, pH 10) of the *o*-methoxyphenol compound **25**. The experimental result was the initial 2e oxidation of the organic part (to the *o*-quinone **26**) at +0.33 V, followed by 1e oxidation of Ni^{II} (to Ni^{III}, **27**) at +0.62 V.[19]

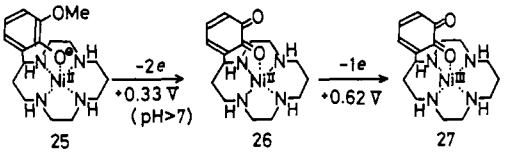

The most dramatic effect by the intramolecular phenolate coordination occurs to the 13-membered N_4 complex **18b**, where the dissociation of the phenol proton transforms the *square-planar* N_4 *low-spin* Ni^{II} complex **18b** (yellow, λ_{max} 424 nm, ϵ 130) into the *folded* N_4 *high-spin* Ni^{II} complex **19b** (pink, λ_{max} 559 n, ϵ 6). Its details were previously reported.[12,13] In 15-membered N_4, Ni^{II} remains a blue, high-spin species with phenolate coordination in **21b** (λ_{max} 576 nm, ϵ 16) or without in **20b** (λ_{max} 551 nm, ϵ 10, at pH 4.3).

Conclusion

Various substituted phenol-pendant 13–15-membered macrocyclic tetraamines (**11a–c**) have been synthesized. The simplicity and versatility of the new annelation method are widely applicable for the synthesis of novel metal chelating agents with various biomimetic functions, as well as of macrocyclic spermine alkaloid analogues. An X-ray crystal structure of the 14-membered cyclam derivative **11b** shows a close proximity of the phenol OH to the macrocyclic ring. The pendant phenols dissociate their protons upon interaction with metal ions Cu^{II}, Ni^{II}, and Fe^{II}, and the resulting phenolate oxygens come to an ideal apical position to be a strong or compulsory fifth donor. The degree of the phenol dissociation varies with metal ions and with macrocyclic ring sizes. Attachment of the intramolecular phenolate coordination makes macrocyclic N_4 species a new class of $Fe^{II,III}$-sequestering agents. Crystal structures of the phenolate-pendant cyclam complexes with Cu^{II} (**11a**) and Ni^{II} (**11b**) disclose the most stable ligand configuration and coordinating-metal characteristics. The 1:1 complexation constant for Cu^{II}–**11b** (in phenolate form) is 1.0×10^{32} M^{-1}, which represents 400 times stability enhancement by the apical phenolate coordination. The apical phenolate anionic donors greatly stabilize Ni^{III} and Fe^{III} encapsulated in macrocyclic N_4, as illustrated by lowered redox potentials for $Ni^{III/II}$ and $Fe^{III/II}$. A good correlation is established between $Ni^{III/II}$ potentials and Hammett σ^* values of substituents on the phenol. The present complexes illustrate the role of apical phenolate (of tyrosine) coordination to favor Fe^{III}– over Fe^{II}–porphyrins in catalase[6] or abnormal hemes.[7]

Acknowledgment. We are grateful to the Ministry of Education for financial assistance (Grant-in-Aid Nos. 60119003 and 61125006).

Supplementary Material Available: Tables of fractional coordinates and isotropic temperature factors, anisotropic temperature factors, bond lengths, and bond angles for the phenol-pendant cyclam and phenolate-pendant cyclam Cu(II) complexes (8 pages); listings of observed and calculated structure factors for the two complexes (18 pages). Ordering information is given on any current masthead page.

(41) Bencini, A.; Fabbrizzi, L.; Poggi, A. *Inorg. Chem.* **1981**, *20*, 2544–2549.
(42) Hine, J. *Physical Organic Chemistry*, 2nd ed.; McGraw-Hill: New York, 1962; pp 81–103.